IOP Publishing Nanotechnology
Nanotechnology 28 (2017) 035707 (7pp) doi:10.1088/1361-6528/28/3/035707

Effect of nanocavities on Ge nanoclustering and out-diffusion in SiO_2

Chen Li[1], Honglei Feng[1], Bin Liu[1], Wenshuang Liang[1], Guiju Liu[1], Guy G Ross[2], Yiqian Wang[1,3] and David Barba[2,3]

[1] College of Physics & The Cultivation Base for State Key Laboratory, Qingdao University, No. 308 Ningxia Road, Qingdao 266071, People's Republic of China
[2] INRS-Énergie, Matériaux et Télécommunications, 1650 boulevard Lionel-Boulet, Varennes, Québec J3X 1S2, Canada

E-mail: yqwang@qdu.edu.cn and barba@emt.inrs.ca

Received 8 September 2016, revised 10 November 2016
Accepted for publication 16 November 2016
Published 14 December 2016

Abstract

Germanium nanocrystals (Ge-ncs) were synthesized by implantation of Ge^+ ions into the fused silica, followed by a thermal annealing at 1000 °C. High-resolution transmission electron microscopy was employed to characterize both the morphology of the formed Ge-ncs and the evolution of their depth-distribution as a function of annealing durations. The formation of nanocavities in the vicinity of nanocrystal/SiO_2 interface is evidenced, as well as their influence on the release of the compressive stress exerted on Ge-ncs by surrounding SiO_2. Some Ge-ncs are found inside nanocavities, and can move into the implanted layer through a nanocavity-assisted diffusion mechanism. This finding sheds light on a new process that can explain the non-uniformity of the Ge-nanocrystal spatial distribution.

Keywords: germanium nanocrystals, thermal diffusion, out-gassing effect, nanocavity, stress relaxation, transmission electron microscopy

(Some figures may appear in colour only in the online journal)

1. Introduction

During last decades, nanostructured germanium (Ge) embedded in silicon dioxide (SiO_2) matrix has received considerable attention because of its potential use as efficient light emitter and its large absorption spectrum in the visible range, which makes it attractive for applications in photonics and photovoltaics [1–5]. A number of techniques have been used to synthesize Ge nanocrystals (Ge-ncs) embedded in SiO_2 matrix, such as thermal oxidation, ion implantation, chemical vapor deposition and co-sputtering [6–9]. Among them, ion implantation technique is very interesting because it enables to control the size and depth-profiles of Ge-ncs in SiO_2 matrix by adjusting the implantation and annealing conditions [7]. However, the poor thermal stability of Ge in silica glass could induce strong Ge outgassing effects for annealing performed above the melting point of Ge (937 °C), which drastically limits the integration of Ge-ncs into optoelectronic devices. During the thermal annealing, the motion of Ge was found to be sensitive to a DC applied voltage [10], as well to the annealing environment [11]. In addition, the Ge desorption can be accompanied by the formation of nanocavities, whose origin and effects on the Ge diffusion mechanism inside SiO_2 are still unclear [7, 10, 12, 13].

Different mechanisms [10–16], involving Ge oxidation at the Ge nanocrystal (Ge-nc)/SiO_2 interface, strong Ge thermal diffusion into the SiO_2 matrix via Ge trapping effects, were proposed, but none of them provided a complete description of the nanocavity formation process supported by observations at atomic scale. In addition, no experimental work can be found regarding the effects of these nanocavities on the inner structure of Ge-ncs, as well as their potential impact on the spatial redistribution of Ge after annealing. However, such investigations are increasingly necessary for controlling the growth of Ge-ncs and their physical properties.

In this paper, the size and depth-distribution of Ge-ncs synthesized at 1000 °C were investigated by transmission

[3] Authors to whom any correspondence should be addressed.

electron microscopy (TEM), which is used to estimate the thermal diffusion coefficient of Ge. High-resolution TEM (HRTEM) images were obtained from the samples annealed for different durations, which is challenging because of the insulator nature of SiO_2. From a careful analysis of the recorded images, we found that both nanocavities and coalesced nanoparticles formed after an annealing of 15 min, demonstrating that the diffusion and the coalescence phenomena affect the microstructure of Ge-ncs. Our HRTEM observations allow us to evidence the formation of nanocavities at Ge-nc/SiO_2 interface, as well as to study the variations of Ge interplanar spacing and stress relaxation effects in several Ge-ncs. It is also demonstrated that Ge-ncs can move into the fused silica matrix through a mechanism assisted by the motion of nanocavities containing inner Ge-ncs, a feature that can strongly affect the Ge depth-profile after annealing.

2. Experimental details

$^{74}Ge^{+}$ ions were implanted into silica slices at an acceleration voltage of 70 kV with a fluence of 8×10^{16} cm^{-2}. After implantation, the samples were annealed at 1000 °C for 15, 30 and 60 min, under high pure nitrogen environment. To avoid any accidental contamination, the gas flux is filtered using an additional nitrogen purifier.

TEM experiments were carried out on specimens prepared for cross-sectional observations using conventional techniques of mechanical polishing and ion thinning. The ion thinning was performed using a Gatan model 691 precision ion polishing system. Selected-area electron diffraction, bright field (BF) and HRTEM imaging were conducted using a JEOL JEM 2100F TEM operated at 200 kV. The Ge depth profiles were calculated using TRIM-SRIM software, taking into account both sputtering and swelling effects [17]. Rutherford backscattering spectroscopy (RBS) measurements were performed with 350 keV $^{4}He^{+}$ ions having a tilt angle of 25° with respect to the sample normal, using a detector mounted at 145° with respect to the incident beam. The RBS spectra deconvolution was carried out using the SIMNRA simulation software [18].

3. Results and discussion

3.1. Ge nanoclustering

Typical cross-sectional BF TEM images are presented in figure 1 for the samples annealed at 1000 °C for 15 min (figure 1(a)), 30 min (figure 1(b)) and 60 min (figure 1(c)). These images were recorded at a same magnification for easy comparison. The dark and bright nano-objects with dimensions between 30 and 60 nm observed in these images correspond to Ge-ncs and nanocavities, respectively. In agreement with previous report [7], the number of nanocavities increases with the annealing duration, as a consequence of Ge outgassing effects. Table 1 presents the average diameters of both Ge-ncs and nanocavities, as well as the Ge concentration obtained from TEM images for each sample. These concentrations were extracted using the bulk concentration of Ge (4.43×10^{22} at cm^{-3}) to evaluate the quantity of Ge in Ge-ncs. The values are underestimated because nanocrystals smaller than 1–2 nm cannot be observed by TEM, neither Ge-ncs that do not satisfy the Bragg diffraction conditions. The data presented in the second and fourth columns of table 1 indicate that both the size and the concentration of remaining Ge in the samples decrease with the annealing duration, while the size of the formed nanocavities reported in the third column increases continuously. These features are a direct consequence of high thermal diffusion of Ge inside fused silica [4], which is responsible for the Ge desorption [7].

All the formed nano-objects are not uniformly distributed in depth within the SiO_2 matrix. As for Si-ncs and Ge-ncs produced by ion implantation into fused silica [7, 19–22], they are size-selectively distributed within the implanted layer. The SRIM-TRIM depth-profile of implanted Ge ions is presented figure 2. These measurements indicate that the biggest nano-objects observed in figures 1(a)–(c) are located in the region where the concentration of implanted Ge is the highest, namely for depths between 20 and 40 nm in all the studied samples.

RBS analysis is used to determine the depth-distribution of Ge inside SiO_2, including isolated Ge atoms that cannot be detected by TEM. By comparing the depth-profile of remaining Ge obtained from TEM observations with that obtained from RBS measurement in figure 2 [7], we can estimate the fraction of Ge involved in the nucleation process. This ratio was found to be around 80% for each sample and independent of the annealing time. In agreement with previous estimations [7, 19, 22], this shows that most of the Ge ions introduced into the fused silica matrix have precipitated during the thermal annealing.

3.2. Ge-nc inner structure and nanocavity formation

Figure 3 shows typical cross-sectional HRTEM images of Ge-ncs and nanocavities formed in the fused silica after an annealing of 15 and 60 min. Figure 3(a) presents a single and isolated Ge-nc with a diameter of about 10 nm, which is well-ordered and almost spherical. A nanoparticle with a diameter of 30 nm is observed in figure 3(b). It is composed of three crystalline regions whose {111} atomic planes are identified by three pairs of parallel lines. Similar structures of several crystallites with different crystal orientations are systematically observed for Ge nanoparticles bigger than 20 nm. Figure 3(c) shows a complete and isolated nanocavity with a diameter of 8 nm, formed after the annealing of 15 min. This cavity results from a complete Ge out-diffusion of a small Ge-nc during the first 15 min of the annealing. Figure 3(d) illustrates a nanoparticle formed after an annealing of 60 min, which is composed of one Ge-nc (area I) and one nanocavity (area II) with diameters of 21 nm and 16 nm, respectively. The cavities observed after an annealing of 60 min are generally bigger than those formed for shorter annealing

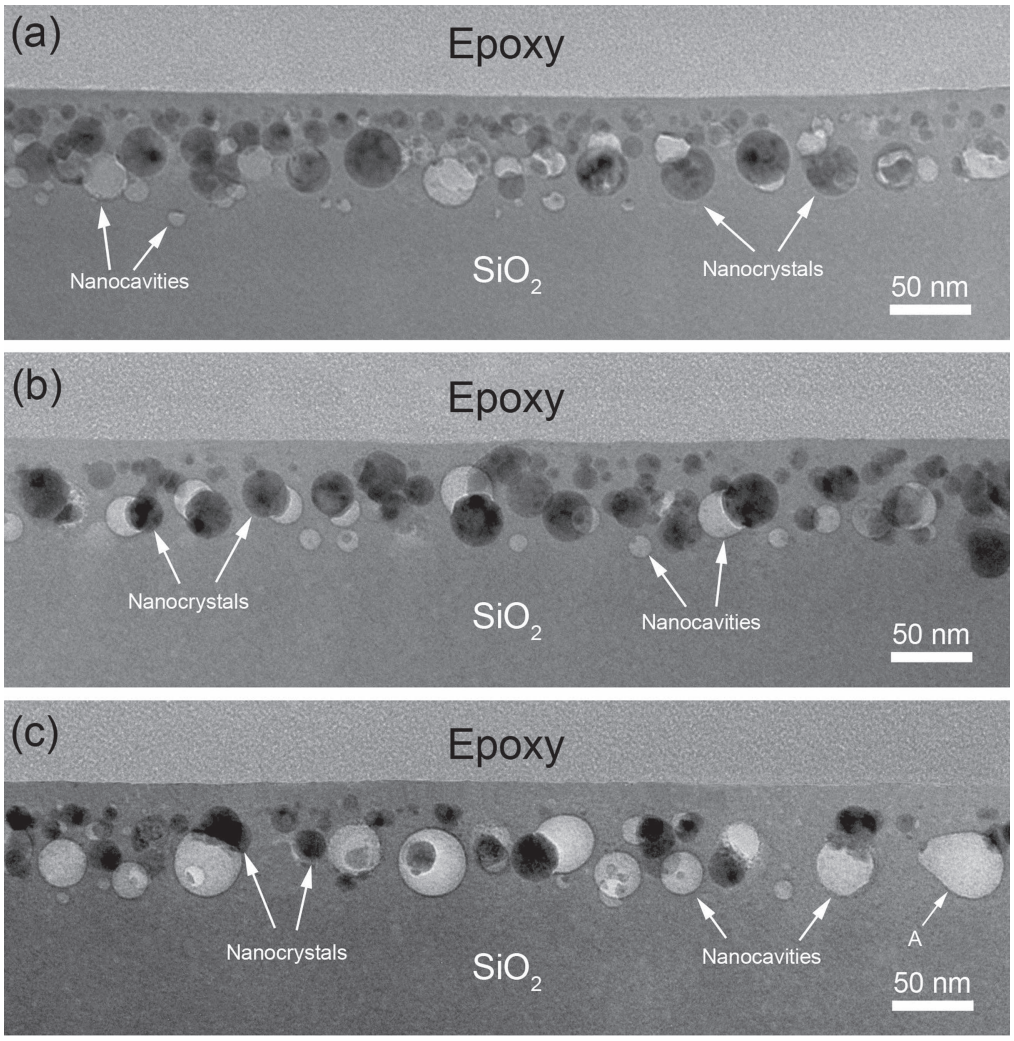

Figure 1. Cross-sectional TEM images of samples annealed for 15 min (a), 30 min (b) and 60 min (c).

Table 1. Evolution of Ge-nc and nanocavity dimensions as a function of annealing times, with corresponding Ge and interplanar spacings measured by TEM.

	Average size (nm)			
Annealing time (min)	Ge-ncs	Nanocavities	Ge concentration (at cm^{-3})	Interplanar spacing (nm)
15	19.46	17.51	3.5×10^{21}	0.313
30	18.14	18.53	2.2×10^{21}	0.316
60	16.10	26.66	1.5×10^{21}	0.320

durations. Regarding the synthesized Ge-ncs, we infer that the spherical and well-ordered nanoparticles smaller than 10 nm are mainly produced by Ostwald ripening [22, 23], a growth process where diffusing Ge atoms aggregate to form isolated clusters, whose dimensions increase with both annealing time and local Ge concentration. On the other hand, large and complex aggregates containing crystallites with different crystal orientations originate from the coalescence of small Ge-ncs. This effect occurs when the spacing between the formed Ge-ncs becomes smaller than their diameters, and it is promoted in the regions where the concentration of implanted Ge is elevated, as well as in the samples annealed for longer durations.

Furthermore, volume expansion effects related to the liquid–solid phase transition of clustered Ge at 938 °C during the sample cooling, lead to the development of mechanical compressive stress inside Ge-ncs [22]. The lattice spacing is measured to be 3.16 ± 0.01 Å for the planes marked by parallel white lines in figure 4(a), which is smaller than that of {111} planes in bulk Ge ($d_{111} = 3.27$ Å). The decrease of (111) lattice spacing reveals a compressive stress of ~3%, which is compatible with the values of 1.5%–4.0%, measured for Ge-ncs synthesized within thin thermal silicon oxide

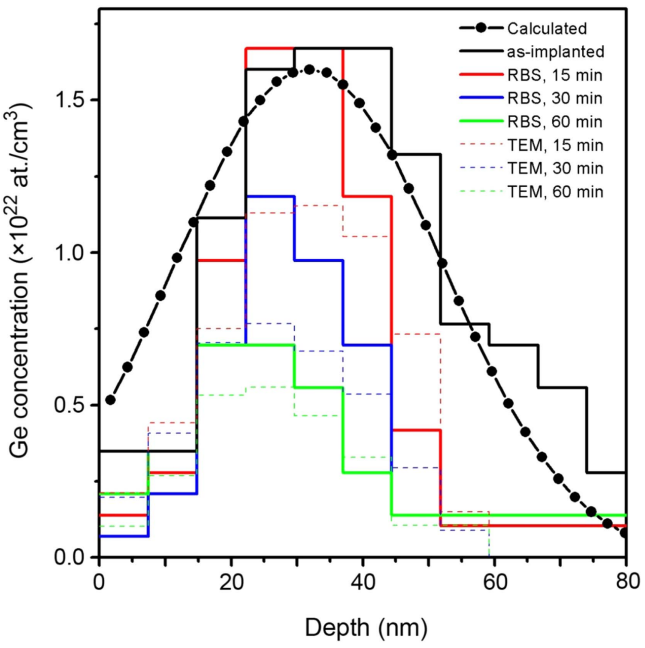

Figure 2. Ge implantation profile calculated from SRIM (curve), RBS depth-profiles of as-implanted and annealed samples (solid lines) (Reprinted with permission from [7]. Copyright 2012 *Institute of Physics Publishing*), and depth-profiles extracted from TEM observations (dashed lines).

layers on Si substrates [22]. For the coalesced Ge-ncs, which are made of agglomerated crystalline regions with different orientations, the internal strain field exerted by the surrounding SiO_2 matrix can be non-uniform. Figure 4(b) shows a nanoparticle synthesized after annealing of 30 min, which is composed of a central amorphous cluster (marked A), surrounded by five crystalline regions (marked I to V). The region labeled I, oriented perpendicular to the Ge-nc radial direction, has an interplanar {111} spacing of 3.15 ± 0.01 Å. For the regions labeled II to V with atomic planes nearly parallel to the Ge-nc radial direction, the {111} lattice spacing is 3.23 Å, 3.20 Å, 3.22 Å and 3.18 Å, respectively. We infer that in such a large Ge nanoparticle, the pressure exerted by the host matrix can be sufficient to prevent the complete crystallization of the Ge core (region A). This scenario is supported by recent work on pressure-induced effects in nanostructured Ge [24], indicating that the Ge–Ge bond compression can give rise to the amorphorization of Ge-ncs. Figure 4(c) shows a third kind of Ge-ncs, which is composed of a Ge-nc from which Ge has partially out-diffused. The release of Ge atoms from Ge-nc is evidenced by the observation of a bright region at its bottom, showing the presence of an inner nanocavity. The formation of such cavities at the Ge-nc boundary is consistent with the mechanism of void formation proposed by Heinig *et al* [11], who correlated this phenomenon with the oxidation of Ge in the vicinity of the

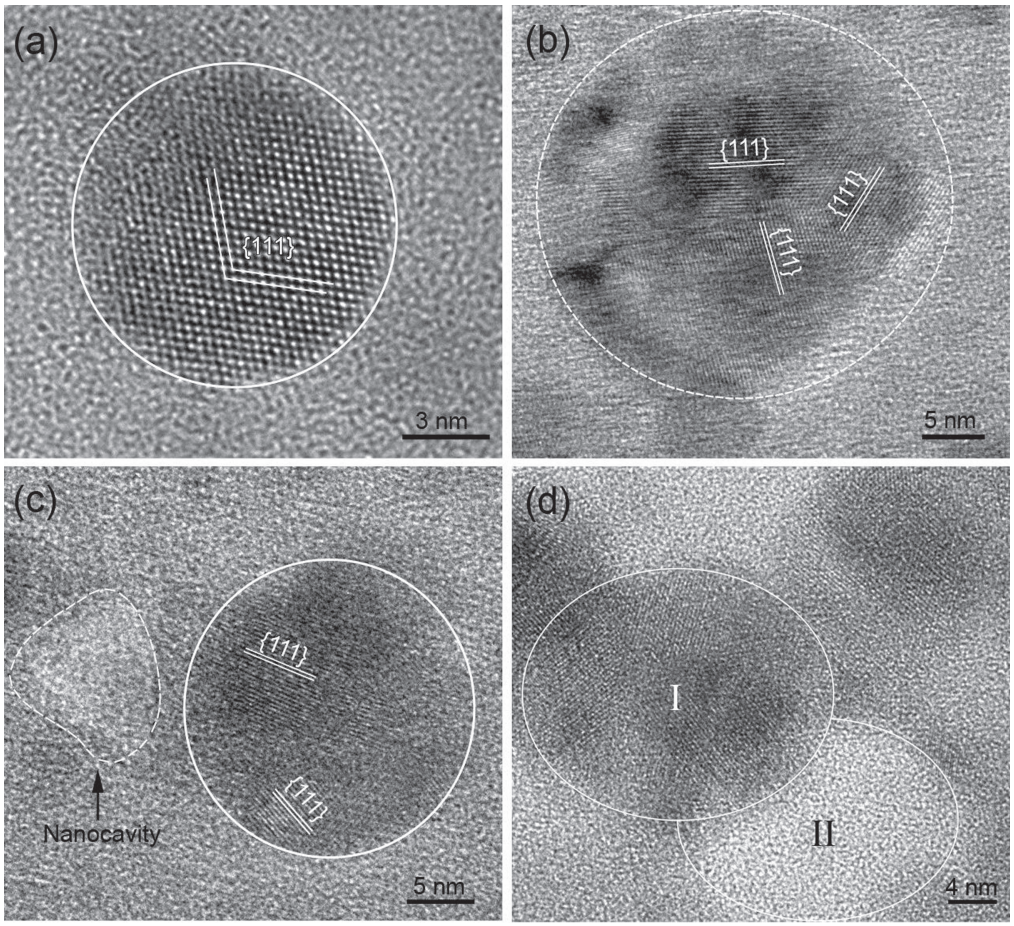

Figure 3. HRTEM images of an isolated Ge-nc (a), a coalesced Ge-nc (b) and an isolated nanocluster produced after an annealing of 15 min, as well as Ge nanoclusters with adjacent nanocavity observed after an annealing of 60 min (d).

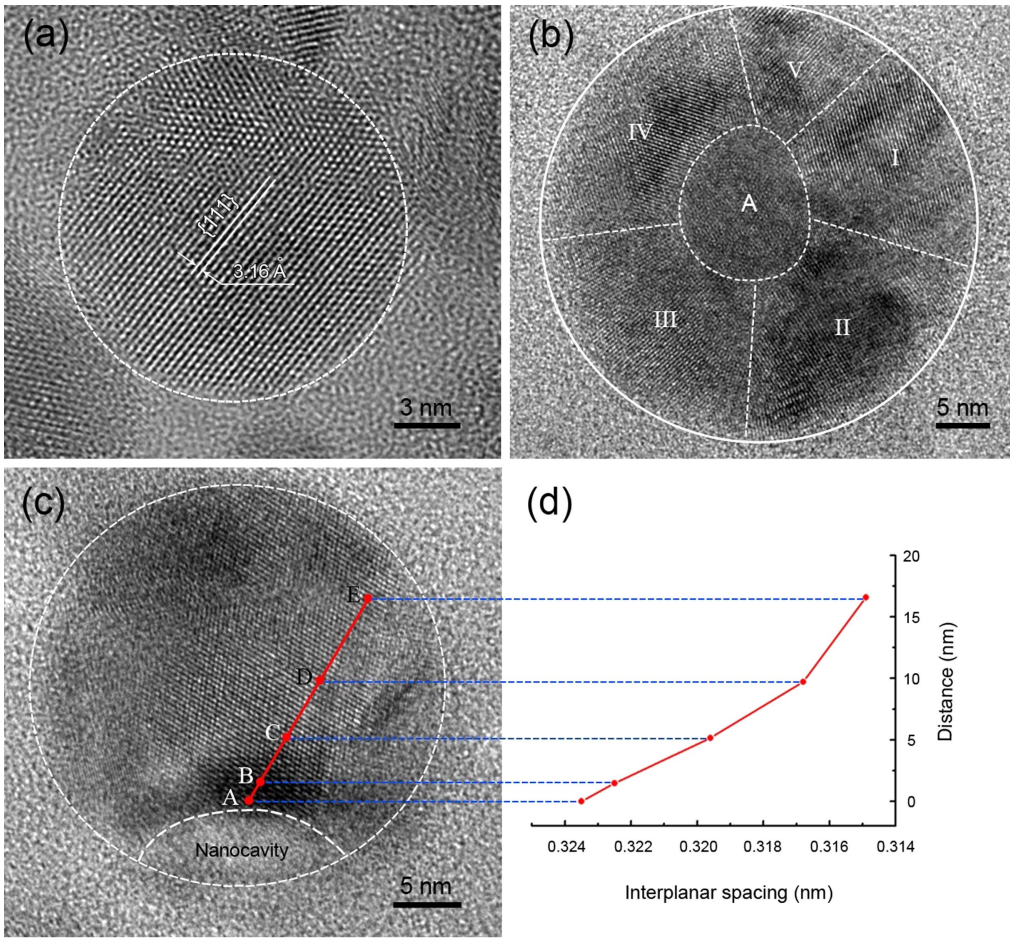

Figure 4. HRTEM images of Ge-ncs with annealing time of 30 min (a) a single nanocrystal, (b) coalesced nanocrystal, and (c) Ge-nc containing a nanocavity, accompanied by the variation of the Ge interplanar spacing measured along the red line (d).

Ge-nc/SiO_2 interface. Due to the kinetics of the chemical reaction, the volume occupied by these nanocavities should increase over annealing time, an effect that is clearly observed when we compare the dimensions of nanocavities observed in figures 1(a) and (c) (bright objects). In order to evaluate the impact of this void on the internal strain field, we measured the interplanar spacing of single Ge-ncs within each sample. The obtained values, reported in the last column of table 1, indicate that the formation of nanocavities is accompanied by a significant reduction of the average strain field inside Ge-ncs. In figure 4(c), we measured the {111} spacing in the nanoparticle where an inner nanocavity is observed. These data are obtained at five different points (labeled A to E) along the red line oriented perpendicular to the lattice planes. The data in figure 4(d) clearly show that the interplanar spacing increases in the vicinity of the inner nanocavity. This suggests that the presence of inner nanocavities releases the compressive stress exerted by the SiO_2 matrix on Ge-ncs, thus contributing to relax their excess energy inside the samples [21].

3.3. Non-uniform Ge-nc depth-distribution

The data in figure 2 show the evolution of the Ge depth-profile as a function of annealing time, $C(z, t)$, which can be used to estimate the thermal diffusion coefficient (D_T) of Ge at a temperature T, using the second Fick's law,

$$\mathrm{Ln}\, C(z, t) = A - \frac{z^2}{4D_T t}, \qquad (1)$$

where z is the depth measured from sample surface, t is the annealing time, $C(z, t)$ is the Ge concentration, and A is a constant. For an annealing duration of 60 min at 1000 °C, we obtained $D_{1000} \sim 10^{-17} - 10^{-16}\,\mathrm{cm^2\,s^{-1}}$. Such a diffusion coefficient is compatible with the data reported in the literature [10, 11, 13]. However, it corresponds to an average diffusion length ($d = \sqrt{D_T t}$) less than one nanometer. This length is insufficient to explain the release of Ge from the samples, which implies Ge displacements over 20–25 nm, as measured from figure 2, between the position of the Gaussian Ge depth-profile, right after ion implantation (as-implanted sample) and after an annealing of 1 h. For such Ge motions, the diffusion coefficient should be 1 or 2 orders of magnitude higher than the one ($10^{-17} - 10^{-16}\,\mathrm{cm^2\,s^{-1}}$) determined using equation (1).

Moreover, in a classical thermal diffusion frame, the Ge distribution after annealing should be more uniform in depth, and not be preferentially oriented towards the top surface of the sample, even if the local damage induced by ion implantation reduces the Ge mobility in the vicinity of sample

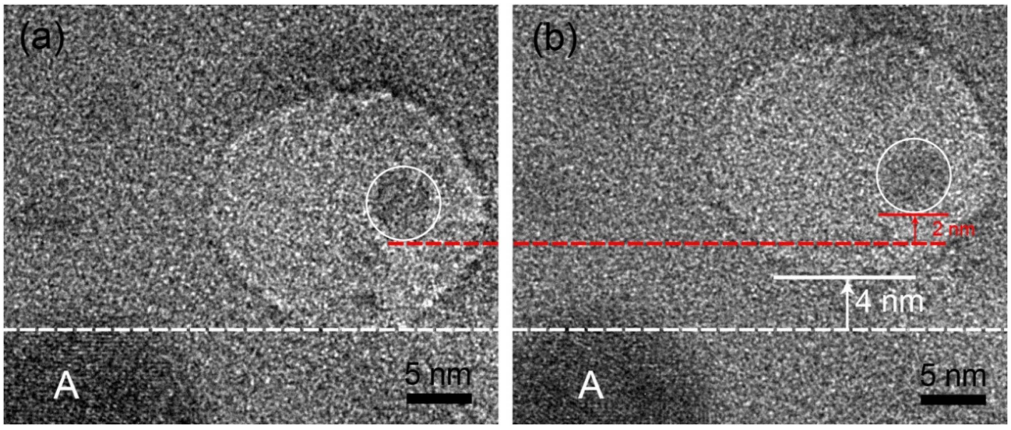

Figure 5. HRTEM images of a nanocavity annealed for 60 min (a) and after electron-beam irradiation for 60 s (b).

surface [7, 16, 22, 25]. Here, it is found that significant decrease of Ge concentration beyond depths of 40 nm in the samples annealed for 30 and 60 min can be associated with the presence of nanocavities (figures 1(b) and (c)). Such a feature may partially result from the lower concentration of silicon dangling bonds induced by ion bombardment at greater depths in the implanted layer, which can locally improve the Ge diffusion, as well as their release from the coalesced nanoparticles [22, 25]. Nevertheless, such a reduction of Ge thermal diffusion in specific sample regions cannot explain the spatial redistribution of Ge after annealing over whole implanted layer.

Last but not the least, we also observe Ge-ncs from which Ge atoms have almost completely out-diffused. These nano-objects are made of small dark clusters embedded into large bright nanocavities (figure 1). One of them is presented at higher magnification in figure 5. Under 200 kV electron-beam irradiation at a current density of ~100–200 pA cm^{-2} for 60 s, we found that both the nanocavity and the Ge-nc have moved. Structural changes induced by intense electron beam in Ge-nc/SiO_2 systems have already been reported, notably by showing that Ge can nucleate or voids can be gradually filled by the migration of O, Si and Ge from the surrounding [11, 26]. Nevertheless, none of these studies has evidenced the occurrence of a Ge diffusion mechanism assisted by the migration of nanocavities containing inner Ge-ncs. The Ge-nc marked by A is motionless (figure 5(a)), so that it can be used as a reference position to measure the relative displacements. The displacement is 4 nm and 2 nm (figure 5(b)) for the nanocavity and the Ge-nc embedded in this nanocavity, respectively. The slower motion of inner Ge-nc with respect to the nanocavity may result from its mass. According to the second Fick's law, the diffusion coefficient related to the displacement of the inner Ge-nc under electron-beam exposure is $\sim 6.7 \times 10^{-16}\,cm^2\,s^{-1}$, which is several times higher than the Ge diffusion coefficient ($\sim 10^{-17} - 10^{-16}\,cm^2\,s^{-1}$) at 1000 °C in the fused silica. Considering that the sample is heated up to a temperature of ~300 °C during the e-beam exposure, we believe that such a nanocavity-assisted Ge-nc diffusion could play an important role during thermal annealing at 1000 °C. As a direct consequence of the high thermal diffusion coefficient associated with this process, this can greatly contribute to the variation of both Ge and void concentrations over the whole implanted layer. For example, the large spherical nanocavities observed close to the center of the implanted layer in figure 1(c) may originate from the coalescence of small nanocavities formed in deeper sample regions, which have diffused over 10–20 nm. This also provides a new global understanding of the depth-profile evolution shown in figure 2. The release of Ge from the regions deeper than 40 nm, where a number of nanocavities was found during the 15 min annealing (figure 1(a)), may result from the displacement of Ge-ncs embedded in nanocavities towards the sample surface. According to the mechanism proposed by Heinig *et al* [11], who suggested the presence of Ge oxide inside the formed nanocavities, the motion of nanocavities containing Ge-ncs is compatible with the work of Beyer and von Borany [13], who attributed the enhanced Ge diffusion and the Ge outgassing to the formation of highly mobile and volatile GeO molecules inside SiO_2. Hence, the Ge spatial redistribution observed after each annealing would result from a Ge thermal diffusion that is almost uniform in depth, and a nanocavity-assisted Ge-nc diffusion process that is preferentially oriented towards the sample surface.

4. Conclusions

In summary, TEM observations of Ge-ncs produced by ion implantation in the fused silica show that both the concentration and the size of the formed Ge nanoclusters decrease continuously with the annealing time. During thermal treatments, inner nanocavities form at the interface between Ge-ncs and the surrounding SiO_2, which contributes to release the compressive stress inside the formed Ge-ncs. The size of these nanocavities increases over time, leading to the formation of nanostructures composed of small Ge-ncs embedded in nanocavities. HRTEM observations show that these inner Ge-ncs can migrate in SiO_2 under electron beam exposure. Their high mobility suggests the occurrence of nanocavity-assisted Ge-nc diffusion mechanisms during

thermal annealing conducted at high temperatures. In addition to improving the thermal diffusion of Ge, this process can strongly affect the Ge depth-profile for long annealing durations. This could explain the displacement of Ge-ncs towards the sample surface by an inhomogeneous migration of nanocavities containing Ge-ncs and/or germanium oxide.

Acknowledgments

The authors would like to thank the financial support from the National Key Basic Research Development Program of China (Grant no.: 2012CB722705), the Natural Science Foundation for Outstanding Young Scientists in Shandong Province, China (Grant no.: JQ201002), High-end Foreign Experts Recruitment Program (Grant nos.: GDW20163500110, GDW20143500163), and the 4th Workgroup Québec-Shandong Program (Grant no.: 190385014). Y Q Wang would also like to thank the financial support from the Top-notch Innovative Talent Program of Qingdao City (Grant no.: 13-CX-8), and the Taishan Scholar Program of Shandong Province, China.

References

[1] Beard M C, Knutsen K P, Yu P, Luther J M, Song Q, Metzger W K, Ellingson R J and Nozik A J 2007 *Nano Lett.* **7** 2506
[2] Trinh M T, Limpens R, de Boer W D A M, Schins J M, Siebbeles L D A and Gregorkiewicz T 2012 *Nat. Photon.* **6** 316
[3] Liu Z, Yang M, Chen T P, Liu Y and Zhang H 2015 *Mater. Des.* **83** 713
[4] Heng C L, Finstad T G, Li Y J, Gunnæs A E, Olsen A and Storas P 2005 *Microelectron. J.* **36** 531
[5] Kan E W H, Chim W K, Lee C H, Choi W K and Ng T H 2004 *Appl. Phys. Lett.* **85** 2349
[6] Baron T, Pelissier B, Perniola L, Mazen F, Hartmann J M and Rolland G 2003 *Appl. Phys. Lett.* **83** 1444
[7] Barba D, Martin F, Demarche J, Terwagne G and Ross G G 2012 *Nanotechnology* **23** 145701
[8] Shen J K, Wu X L, Bao X M, Yuan R K, Zou J P and Tan C 2000 *Phys. Lett.* A **273** 208
[9] Peibst R, Dürkop T, Bugiel E, Fissel A, Costina I and Hofmann K R 2009 *Phys. Rev.* B **79** 195316
[10] Minke M V and Jackson K A 2005 *J. Non-Cryst. Solids* **351** 2310
[11] Heinig K H, Schmidt B, Markwitz A, Grotzschel R, Strobel M and Oswald S 1999 *Nucl. Instrum. Methods* B **148** 969
[12] Markwitz A, Schmidt B, Matz W, Grötzschel R and Mücklich A 1998 *Nucl. Instrum. Methods* B **142** 338
[13] Beyer V and von Borany J 2008 *Phys. Rev.* B **77** 014107
[14] Baranwal V, Gerlach J W, Lotnyk A, Rauschenbach B, Karl H, Ojha S, Avasthi D K, Kanjilal D and Pandey A C 2015 *J. Appl. Phys.* **118** 134303
[15] Xue Z Y, Di Z F, Ye L B, Mu Z Q, Chen D, Wei X, Zhang M and Wang X 2014 *Thin Solid Films* **557** 120
[16] Barba D, Demarche J, Martin F, Terwagne G and Ross G G 2012 *Appl. Phys. Lett.* **101** 143107
[17] Ziegler J F, Ziegler M D and Biersack J P 2010 *Nucl. Instrum. Methods* B **268** 1818
[18] Mayer M 1997 *SIMNRA User's Guide Report* IPP 9/113 Max-Planck Institut fur Plasmaphysik, Garching
[19] Barba D, Demarche J, Martin F, Terwagne G and Ross G G 2013 *J. Appl. Phys.* **114** 074306
[20] Wang Y, Ross G G and Smirani R 2004 *Nanotechnology* **15** 1554
[21] Cai R S, Wang Y Q, Shang L, Liu X H, Zhang Y J, Ross G G and Barba D 2014 *J. Appl. Phys.* **115** 204310
[22] Zhang M, Cai R S, Zhang Y, Wang C, Wang Y Q, Ross G G and Barba D 2014 *Mater. Charact.* **93** 1
[23] Bonafos C, Colombeau B, Altibelli A, Carrada M, Assayag G B, Garrido B, López M, Pérez-Rodríguez A, Morante J R and Claverie A 2001 *Nucl. Instrum. Methods* B **178** 17
[24] Corsini N R C *et al* 2015 *Nano Lett.* **15** 7334
[25] Barba D, Cai R S, Demarche J, Wang Y Q, Terwagne G, Rosei F, Martin F and Ross G G 2014 *Appl. Phys. Lett.* **104** 111901
[26] Klimenkov M, Matz W and von Borany J 2000 *Nucl. Instrum. Methods* B **168** 367